Available online at www.sciencedirect.com
ScienceDirect
Journal of Nuclear Materials 374 (2008) 378–385
journal of nuclear materials
www.elsevier.com/locate/jnucmat

Thermal conductivities of hypostoichiometric (U, Pu, Am)O_{2-x} oxide

Kyoichi Morimoto [a,*], Masato Kato [a], Masahiro Ogasawara [b], Motoaki Kashimura [a]

[a] Nuclear Fuel Cycle Engineering Laboratories, Japan Atomic Energy Agency, 4-33 Muramatsu, Tokai-mura, Naka-gun, Ibaraki 319-1194, Japan
[b] Inspection Development Company, 4-33 Muramatsu, Tokai-mura, Naka-gun, Ibaraki 319-1194, Japan

Received 26 May 2007; accepted 14 September 2007

Abstract

The thermal conductivities of $(U_{0.68}Pu_{0.30}Am_{0.02})O_{2.00-x}$ solid solutions ($x = 0.00$–0.08) were studied at temperatures from 900 to 1773 K. The thermal conductivities were obtained from the thermal diffusivities measured by the laser flash method. The thermal conductivities obtained experimentally up to about 1400 K could be expressed by a classical phonon transport model, $\lambda = (A + BT)^{-1}$, $A(x) = 3.31 \times x + 9.92 \times 10^{-3}$ (mK/W) and $B(x) = (-6.68 \times x + 2.46) \times 10^{-4}$ (m/W). The experimental A values showed a good agreement with theoretical predictions, but the experimental B values showed not so good agreement with the theoretical ones in the low O/M ratio region. From the comparison of A and B values obtained in this study with the ones of $(U,Pu)O_{2-x}$ obtained by Duriez et al. [C. Duriez, J.P. Alessandri, T. Gervais, Y. Philipponneau, J. Nucl. Mater. 277 (2000) 143], the addition of Am into (U, Pu)O_{2-x} gave no significant effect on the O/M dependency of A and B values.

PACS: 66.70.+f; 66.30.Xj

1. Introduction

Thermal conductivity of nuclear fuel is one of the most important properties for design and performance analyses of fuel rods. Many studies [1–11] have been done on the thermal conductivities of uranium dioxide (UO_2) and uranium–plutonium mixed oxide (MOX) fuels and some reviews [12,13] have also been published. The effect of oxygen-to-metal ratio (O/M ratio) on the thermal conductivity has been pointed out in these reviews.

When recycling of MOX fuel is repeated in a fast breeder reactor (FBR), MOX fuel contains a considerable amount of ^{241}Pu, which has a half-life of 14.4 years. Consequently, its daughter nuclide ^{241}Am builds up in the MOX fuel with time. If the storage time between reprocessing of irradiated fuel and MOX fuel loading into the reactor becomes long, a considerable amount of ^{241}Am accumulates in the MOX fuel, and affects its thermal and mechanical properties. However, there has been no study on the effects of Am content on the thermal conductivity of MOX fuel except for our study in which we reported that the thermal conductivities of MOX fuel containing a few percent of Am decreased slightly with increasing Am-content [14].

In this study, we prepared MOX fuels containing Am and measured their thermal conductivities as a function of the O/M ratio in the range from 2.00 to 1.92. These results were discussed, based on a theory of classical phonon scattering.

2. Experimental

2.1. Preparation of specimens

The specimens used in this study were $(U_{0.68}Pu_{0.30}Am_{0.02})O_{2.00-x}$ (2%Am–MOX, $x = 0.00$–0.08) pellets. The content of Pu was nearly 30% of the total metal content and that of Am was about 2.2%. Preparation details for

* Corresponding author. Tel.: +81 29 282 1111; fax: +81 29 282 9473.
E-mail address: morimoto.kyoichi@jaea.go.jp (K. Morimoto).

0022-3115/$ - see front matter © 2007 Elsevier B.V. All rights reserved.
doi:10.1016/j.jnucmat.2007.09.003

stoichiometric 2%Am–MOX have been described elsewhere [14].

The adjustments of O/M ratio of specimens to 2.00 were done as follows. First, the O/M ratios of all specimens were conditioned to be 2.00 by heating them in a furnace at 1123 K for 5 h under a flowing atmosphere of Ar–5%H_2 mixed gas containing a suitable amount of moisture. The oxygen potential of the furnace atmosphere was measured at both inlet and outlet for the flowing gas using an oxygen sensor with a stabilized zirconia solid electrolyte. The oxygen potential was controlled to −420 kJ/mol by changing the amount of moisture in the atmosphere so that it corresponded to the stoichiometric composition (O/M = 2.00) in the specimen. The specimen weights were measured at room temperature and used as the basis for the determination of O/M ratio in the hypostoichiometric specimens, as described later.

The main specimen impurities are listed in Table 1 and other characteristics are listed in Table 2. X-ray diffraction measurements (X-ray diffractometer RINT-1100, Rigaku Co. Ltd.) were made on a stoichiometric specimen after crushing it to powder. As shown in Fig. 1, the diffraction patterns of this specimen indicate that it has a single phase with fluorite structure. The lattice parameter calculated from the diffraction patterns is shown in Fig. 2 and is in good agreement with the value predicted using Vegard's law [15]. It was, thus, confirmed that the O/M ratio of this specimen was 2.00.

Table 1
Impurity analysis results of sample taken from the specimens

Element	Concentration (ppm)
Ag	<5
Al	<100
B	<5
Cd	<5
Cr	<50
Cu	<10
Fe	<100
Mg	<15
Mn	<20
Ni	<50
Si	<100
V	<50
Zn	<100
Ca	<30
Pb	<30
Sn	<30
Mo	<50
Na	80

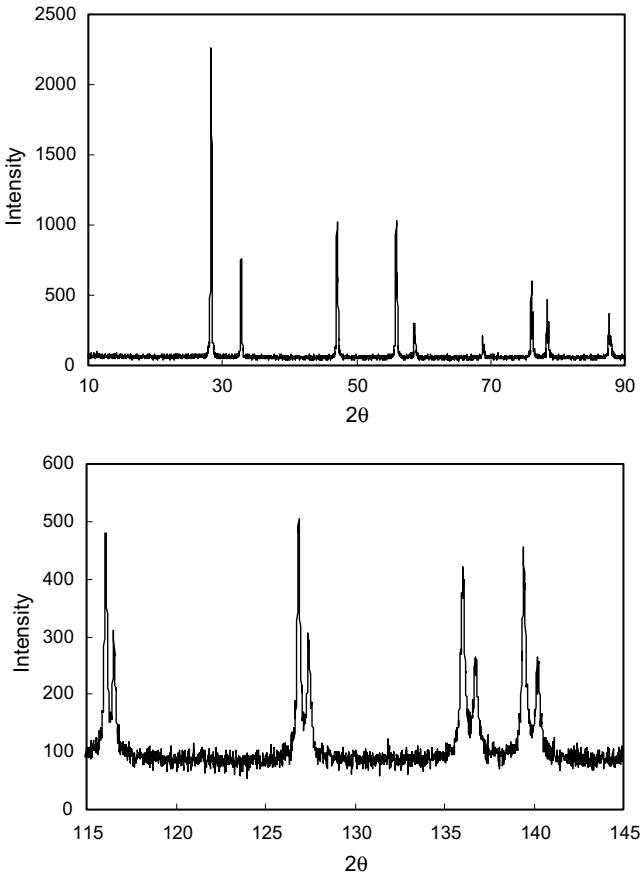

Fig. 1. The diffraction patterns of stoichiometric specimen.

The stoichiometric specimen was cold-mounted in araldite, and its transverse cross section was mirror-polished. The cross section microstructure was observed with an optical microscope (Union Optical Co. Ltd.), and its element distribution was analyzed with an electron probe microanalyzer (EPMA; JXA-8800, JEOL Ltd.). It was shown from the microstructure observation in Fig. 3 that the pores were dispersed uniformly. As shown from the EPMA mapping results in Fig. 4, the specimen had a high degree of homogeneity, and there was no segregation among the constituent elements.

The hypostoichiometric specimens ($U_{0.68}Pu_{0.30}Am_{0.02})O_{2.00-x}$ were prepared by changing both the

Table 2
Main characteristics of the specimens

Specimen no.	Pu/(U + Pu + Am) (mol%)	Am/(U + Pu + Am) (mol%)	Theoretical density (%TD)	Specimen weight (g)	Diameter (mm)	Thickness (mm)
OM-1	29.52	2.19	93.6	0.270	5.71	1.02
OM-2			94.2	0.274	5.48	1.16
OM-3			93.9	0.273	5.48	1.10
OM-4			94.2	0.285	5.52	1.16
OM-5			93.4	0.271	5.50	1.09
OM-6			93.1	0.264	5.51	1.07

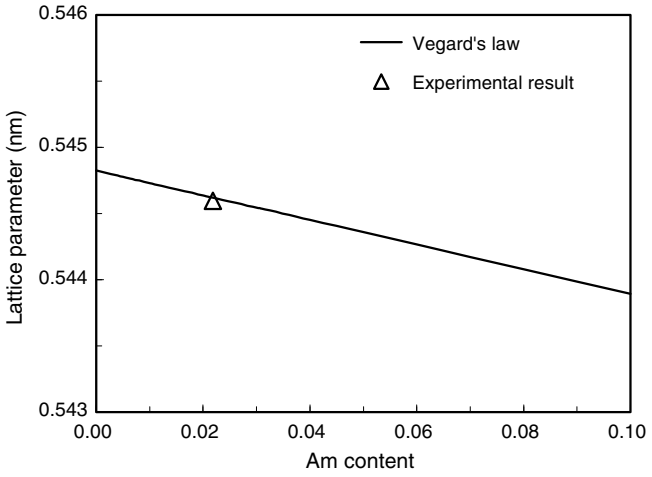

Fig. 2. Lattice parameter of stoichiometric specimen as a function of the Am content. The triangle is the experimental value. The solid line is for the lattice parameter of the $(U_{0.70-z}Pu_{0.30}Am_z)O_2$ solid solution calculated from Vegard's law.

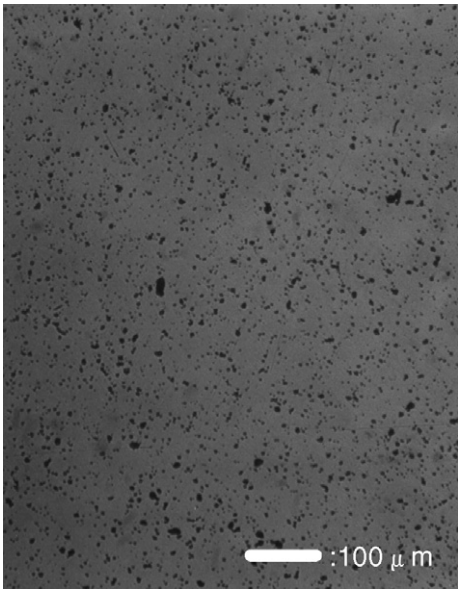

Fig. 3. Ceramography result of the cross section of stoichiometric specimen.

Table 3
Heating conditions for adjusting O/M ratio

Specimen no.	O/M ratio	Temperature (K)	Oxygen partial pressure (atm)
OM-1	2.000	1123	2.045×10^{-20}
OM-2	1.982	1673	2.907×10^{-15}
OM-3	1.961	1773	2.155×10^{-14}
OM-4	1.944	1873	1.123×10^{-13}
OM-5	1.919	1988	3.071×10^{-13}
OM-6	1.903	2016	3.072×10^{-13}

moisture and temperature in the furnace. Table 3 shows the O/M ratios and the heating conditions of each specimen. The O/M ratios of specimens were gravimetrically determined from the weight change between the stoichiometric and hypostoichiometric specimens at room temperature.

2.2. Thermal diffusivity measurements

The thermal diffusivities of specimens were measured at temperatures from 900 to 1773 K with a laser flash apparatus (TC-7000UVH, ULVAC-RIKO Co. Ltd.). Details of this have been described elsewhere [14]. Thermal diffusivities were measured three times at each temperature and were averaged. Thermal diffusivities were calculated from recorded data by the curve-fitting method [16]. The thermal expansion of specimen thickness during the measurements was taken into consideration by using the equation reviewed by Carbajo et al. [13] for determining the thermal diffusivity. Reliability of the thermal conductivity measurements was examined by confirming that the thermal conductivity of UO_2 obtained in this study agreed fairly with thermal conductivities reviewed by Carbajo et al. [13]. Details of this result were described previously [14].

After the thermal diffusivity measurements, the O/M ratios of specimens were measured again by using a thermogravimetric-differential thermal analyzer (TG-DTA) (TG8120 of Rigaku Co. Ltd.). These results are shown in Table 4. There are slightly appreciable differences in O/M ratios before and after thermal diffusivity measurements. Then, the average value of these O/M ratios was adopted as the one in thermal diffusivity measurement.

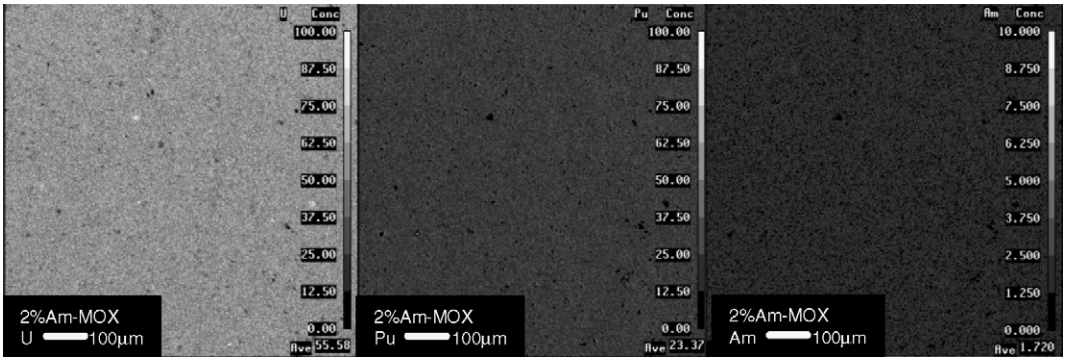

Fig. 4. EPMA mapping results of the cross section of stoichiometric specimen.

Table 4
Variation of O/M ratios before and after thermal diffusivity measurements

Specimen no.	O/M ratio		
	Before	After	Average
OM-1	2.000	1.998	1.999
OM-2	1.982	1.976	1.979
OM-3	1.961	1.964	1.963
OM-4	1.944	1.948	1.946
OM-5	1.919	1.924	1.922
OM-6	1.903	1.926	1.915

2.3. Thermal conductivity calculation

The thermal conductivity data were calculated from thermal diffusivity measurements by the following equation:

$$\lambda(T) = \alpha(T)\rho(T)C_p(T), \tag{1}$$

where $\alpha(T)$ is thermal diffusivity, $C_p(T)$ the heat capacity at constant pressure and $\rho(T)$ density of the specimen. The density of $(U_{0.68}Pu_{0.30}Am_{0.02})O_{2-x}$ was evaluated by the following equation:

$$\rho_{2-x} = \frac{W_{2-x}}{V_{2.00} \times \left(\frac{a_{2-x}}{a_{2.00}}\right)^3}, \tag{2}$$

where W_{2-x} is the weight of $(U_{0.68}Pu_{0.30}Am_{0.02})O_{2-x}$ specimen, $V_{2.00}$ the volume of stoichiometric specimen at room temperature, $a_{2.00}$ lattice parameter of stoichiometric specimen and a_{2-x} lattice parameter of hypostoichiometric specimen predicted by Kato et al. [15]. The variation of density by the thermal expansion during the measurement was taken into consideration by using the equation reviewed by Carbajo et al. [13]. The heat capacity of $(U_{0.68}Pu_{0.30}Am_{0.02})O_2$ was estimated by using Kopp's law:

$$C_p[(U_{0.68}Pu_{0.30}Am_{0.02})O_2] = 0.68 \times C_p(UO_2) + 0.3 \times C_p(PuO_2) + 0.02 \times C_p(AmO_2), \tag{3}$$

where $C_p(UO_2)$ [13], $C_p(PuO_2)$ [13] and $C_p(AmO_2)$ [17] are the heat capacities of UO_2, PuO_2 and AmO_2 respectively. The effect of oxygen deficiency on the heat capacity was taken into consideration by subtracting heat capacity of oxygen deficiency:

$$C_p[(U_{0.68}Pu_{0.30}Am_{0.02})O_{2-x}] = C_p[(U_{0.68}Pu_{0.30}Am_{0.02})O_2] - x/2 \times C_p(O_2), \tag{4}$$

where $C_p(O_2)$ are the heat capacities of O_2 [11].

For the porosity effect correction, the modified Maxwell–Eucken relation was used: $F(p) = (1-p)/(1-\beta p)$ where $\beta = 0.5$ was from the result of our previous paper [14]. By using $\lambda = F(p) \times \lambda_0$, we obtained the thermal conductivities λ_0 of a 100% theoretical density fuel from the conductivities λ obtained with a real specimen at porosity p.

3. Results and discussion

3.1. Experimental results

The thermal conductivities of 2%Am–MOX having a different O/M ratio are shown in Fig. 5 as a function of temperature. The thermal conductivities were derived from the thermal diffusivities by using Eq. (1), and then these data were normalized to 100% of the theoretical density by using the modified Maxwell–Eucken relationship mentioned already. This figure indicates that the thermal conductivities of 2%Am–MOX decrease with increasing temperature and larger deviations of O/M ratios from 2.00. The effect of O/M ratio on the thermal conductivity is large and is significant especially in the low temperature region.

The thermal resistivities, the reciprocals of thermal conductivities, of 2%Am–MOX were evaluated based on the classical phonon transport model. Since the thermal resistivities increase linearly with the increase of temperature up to about 1400 K, the thermal conductivities of 2%Am–MOX can be expressed in the temperature region below 1400 K by the following equation:

$$\lambda = (A + BT)^{-1}. \tag{5}$$

The A and B values were determined by fitting the thermal conductivity data to Eq. (5) and are shown in Table 5 and Fig. 6. They can be given by the following expressions:

$$\lambda_0 = 1/(A + BT),$$
$$A(x) = 3.31 \times x + 9.92 \times 10^{-3}\ (\mathrm{mK/W}),$$
$$B(x) = (-6.68 \times x + 2.46) \times 10^{-4}\ (\mathrm{m/W}).$$

The A values increase linearly with increasing x, while the B values decrease slightly with increasing x although the variation is small.

3.2. Lattice defect thermal resistivity

Based on the classical phonon transport model of dielectric solids above their Debye temperature, A in Eq. (5) is

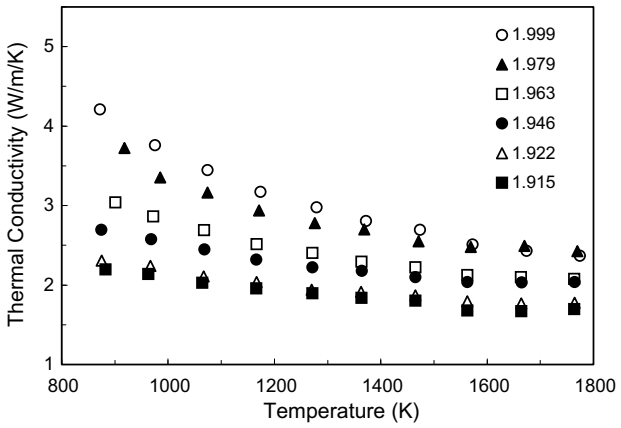

Fig. 5. Thermal conductivities of near-stoichiometric and hypostoichiometric specimens as a function of temperature.

Table 5
A and B values obtained from the results of measurements and calculations

Specimen no.	O/M ratio	A		B	
		Measured values	Calculated values	Measured values	Calculated values
OM-1	1.999	2.776×10^{-2}	2.999×10^{-2}	2.424×10^{-4}	2.306×10^{-4}
OM-2	1.979	6.045×10^{-2}	8.471×10^{-2}	2.350×10^{-4}	2.289×10^{-4}
OM-3	1.963	1.213×10^{-1}	1.287×10^{-1}	2.351×10^{-4}	2.275×10^{-4}
OM-4	1.946	2.062×10^{-1}	1.753×10^{-1}	1.924×10^{-4}	2.261×10^{-4}
OM-5	1.922	2.643×10^{-1}	2.407×10^{-1}	1.981×10^{-4}	2.241×10^{-4}
OM-6	1.915	2.926×10^{-1}	2.597×10^{-1}	1.911×10^{-4}	2.235×10^{-4}

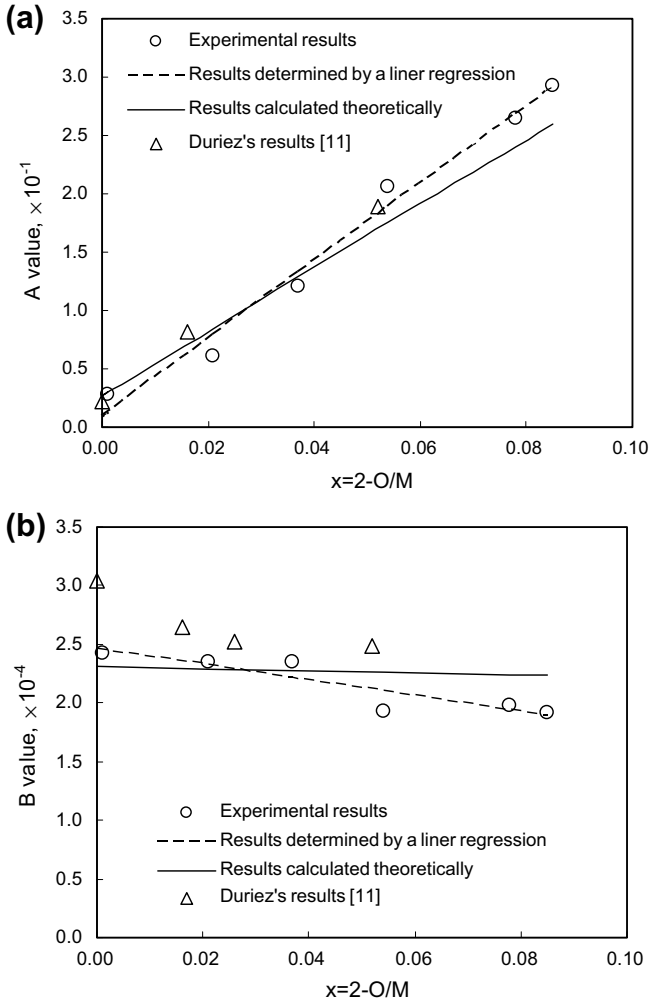

Fig. 6. A and B values as a function of x. (a) Circles are A values obtained from the experimental data. The dashed line shows the result determined by a linear regression of the A values obtained experimentally. The solid line shows the A values calculated theoretically. Triangles are A values reported by Duriez et al. [11]. (b) Circles are B values obtained from the experimental data. The dashed line shows the result determined by a linear regression of the B values obtained experimentally. The solid line shows the B values calculated theoretically. Triangles are B values reported by Duriez et al. [11].

the lattice defect thermal resistivity, due to the interaction of phonons with the lattice defect. BT corresponds to the intrinsic lattice thermal resistivity due to the phonon–phonon interactions based on the Umklapp process.

Based on the Ambegaoker's theory [18], A is represented by the following relationship:

$$A = \frac{\pi^2 \overline{V}\theta}{3\overline{v}^2 h}\sum_i \Gamma_i = C\sum_i \Gamma_i, \tag{6}$$

where $\overline{V}$ is the average atomic volume, θ the Debye temperature, $\overline{v}$ the average phonon velocity, and h Planck's constant. Γ_i is a scattering cross section parameter of phonons by point defect i and is approximately given by the following equation [19]:

$$\Gamma_i = X_i\left[\left(\frac{\overline{M}-M_i}{\overline{M}}\right)^2 + \varepsilon\left(\frac{\overline{r}-r_i}{\overline{r}}\right)^2\right], \tag{7}$$

where X_i and M_i are the atomic fraction and the mass of point defect i, respectively. $\overline{M}$ is the average atomic mass of the host lattice site, r_i the atomic radius of the point defect i in its own lattice, and $\overline{r}$ the average atomic radius of the host lattice site. The parameter ε is one which represents the magnitude of lattice strain generated by the point defect and is obtained by fitting the experimental data to Eq. (7) [19].

The sum of Γ_i is expressed as

$$\sum_i \Gamma_i = \left(\frac{\sum_i X_i M_i^2 - \overline{M}^2}{\overline{M}^2}\right) + \varepsilon\left(\frac{\sum_i X_i r_i^2 - \overline{r}^2}{\overline{r}^2}\right). \tag{8}$$

In this study, the contents of U, Pu and Am in the specimens were about 68%, 30% and 2% respectively. It is known in actinide compounds that U can exist as U^{4+}, U^{5+} and U^{6+}, Pu as Pu^{3+} and Pu^{4+}, and Am as Am^{3+} and Am^{4+}. Thus, many different compositions of cation valence can be predicted in actinide compounds, but we assumed, for present study, as pointed out by Kato et al. [15] that the combination of U^{4+}, Pu^{4+} and Am^{4+} is suitable in the stoichiometric $(U_{0.68}Pu_{0.30}Am_{0.02})O_{2.00}$.

The combinations of actinide ion valences in the lattice change when the oxygen vacancies are generated in the stoichiometric specimen and its O/M ratio decreases. According to thermodynamic studies on the oxygen potential of Am–MOX [20], the oxygen potential in Am–MOX is higher than that in MOX specimens. Thus, Am becomes trivalent more easily than Pu.

As already described, the effect of O/M ratio on the thermal conductivity was investigated in the O/M ratio range from 1.903 to 1.982. We assumed in this O/M ratio

range that all Am^{4+} became Am^{3+} and additionally some Pu^{4+} was converted to Pu^{3+} and new point defects consisting of U^{4+}, Pu^{4+}, Pu^{3+}, Am^{3+}, O^{2-} and O_v (oxygen vacancy) were created in the hypostoichiometric specimens in order to evaluate the influence of O/M ratio on thermal conductivity. The effect of this O/M ratio change on the thermal conductivity has been investigated by several authors [2,4,11,21,22]. According to their analyses, the variation of lattice defect thermal resistivity A can be expressed as follows:

$$\Delta A = A_{2-x} - A_{2.00} = C_{2-x}\sum_j \Gamma_j - C_{2.00}\sum_i \Gamma_i, \tag{9}$$

$$A_{2.00} = C_{2.00}\sum_i \Gamma_j = C_{2.00}\left[\left\{\frac{X_{U^{4+}}M_U^2 + X_{Pu^{4+}}M_{Pu}^2 + X_{Am^{4+}}M_{Am}^2 + X_{O^{2-}}M_{O^{2-}}^2}{\overline{M}_{2.00}^2} - 1\right\} + \varepsilon\left\{\frac{X_{U^{4+}}r_{U^{4+}}^2 + X_{Pu^{4+}}r_{Pu^{4+}}^2 + X_{Am^{4+}}r_{Am^{4+}}^2 + X_{O^{2-}}r_{O^{2-}}^2}{\overline{r}_{2.00}^2} - 1\right\}\right], \tag{14}$$

where ΔA is the difference of A values between the hypostoichiometric oxide and the stoichiometric oxide. The subscripts i and j mean that the sums are for all the point defects of the stoichiometric and hypostoichiometric oxides.

$C_{2.00}$ in Eq. (9) is calculated by

$$C_{2.00} = \frac{\pi^2\overline{V}\theta_{2.00}}{3\overline{v}_{2.00}^2 h} \tag{10}$$

and Debye temperature of Am–MOX is obtained by

$$\frac{\theta_{AmMOX}}{\theta_{UO2}} = \frac{(\overline{M}_{UO_2})^{1/2}(\overline{V}_{UO_2})^{1/3}(T_{M-AmMOX})^{1/2}}{(\overline{M}_{AmMOX})^{1/2}(\overline{V}_{AmMOX})^{1/3}(T_{M-UO_2})^{1/2}}, \tag{11}$$

where T_{M-UO_2} and $T_{M-AmMOX}$ are melting temperatures of UO_2 and Am–MOX, respectively. In this estimation, we used the value of $\theta_{UO_2} = 242$ K reported by Willis [23] and $T_{M-UO_2} = 3138$ K from the experimental result measured by Latta and Fryxel [24]. The melting temperature of Am–MOX, $T_{M-AmMOX}$, is estimated from the data obtained by Kato et al. [25].

The average phonon velocity can be estimated by the following equation derived from the Debye approximation:

$$\overline{v}_{AmMOX} = \overline{v}_{UO_2}\left(\frac{\theta_{AmMOX}}{\theta_{UO_2}}\right)\left(\frac{a_{AmMOX}}{a_{UO_2}}\right), \tag{12}$$

where a_{AmMOX} and a_{UO_2} are lattice parameters of the Am–MOX mentioned in Eq. (2) and UO_2 [24].

C_{2-x} in Eq. (9) is calculated by

$$\frac{C_{2-x}}{C_{2.00}} = \left(\frac{a_{2-x}}{a_{2.00}}\right)^2, \tag{13}$$

where $a_{2.00}$ and a_{2-x} are the lattice parameters of the stoichiometric and hypostoichiometric specimens mentioned in Eq. (2).

The lattice defect thermal resistivity of the stoichiometric specimen, $A_{2.00}$, in Eq. (9) is described as follows:

where $\overline{M}_{2.00}$ is the average atomic mass of the elements contained in Eq. (14) and $\overline{r} = 0.68/3\ r_{U^{4+}} + 0.3/3\ r_{Pu^{4+}} + 0.02/3\ r_{Am^{4+}} + 2/3\ r_{O^{2-}}$.

The ionic radii of cations and anions are shown in Table 6 [26,27].

For the hypostoichiometric specimen, the lattice defect thermal resistivity, A_{2-x}, is described as follows:

$$A_{2-x} = C_{2-x}\sum_i \Gamma_j = C_{2-x}\left[\left\{\frac{X_{U^{4+}}M_U^2 + (X_{Pu^{4+}} + X_{Pu^{3+}})M_{Pu}^2 + X_{Am^{3+}}M_{Am}^2 + X_{O^{2-}}M_{O^{2-}}^2}{\overline{M}_{2-x}^2} - 1\right\} + \varepsilon\left\{\frac{X_{U^{4+}}r_{U^{4+}}^2 + X_{Pu^{4+}}r_{Pu^{4+}}^2 + X_{Pu^{3+}}r_{Pu^{3+}}^2 + X_{Am^{3+}}r_{Am^{3+}}^2 + X_{O^{2-}}r_{O^{2-}}^2 + X_{O_v}r_{O_v}^2}{\overline{r}_{2-x}^2} - 1\right\}\right], \tag{15}$$

where $\overline{M}_{2-x}$ is the average atomic mass of the elements contained in Eq. (15) and $\overline{r} = 0.68/3\ r_{U^{4+}} + (0.32-2x)/3\ r_{Pu^{4+}} + (2x-0.02)/3\ r_{Pu^{3+}} + 0.02/3\ r_{Am^{3+}} + (2-x)/3\ r_{O^{2+}} + x/3\ r_{O_v}$ from electric neutrality and composition of specimen.

The dependency of A values on the deviation of O/M ratios from 2.00 can be theoretically estimated by using the equations from (5)–(15). When $\varepsilon = 49$, both the experimental and the calculated A values show good agreement with each other as indicated in Table 5 and Fig. 6(a). This value is not so different from the $\varepsilon = 55 \pm 50$ for $(U,Pu)O_2$ reported by Fukushima et al. [4], and the $\varepsilon = 42$ for $(U,Pu,Am)O_2$ reported by our previous study [14]. The dependency of A values on O/M ratios obtained in this study was compared with those of $(U,Pu)O_{2-x}$ reported by Duriez et al. [11], although the Pu content in specimens studied by them was up to 15%, and the range of O/M

Table 6
Ionic radii used in this study

Ion		Radius (nm)
Anion	CN = 4	
O^{2-}		0.1368 [26]
O_v		0.1500 [26]
Cation	CN = 8	
U^{4+}		0.1001 [26]
U^{5+}		0.0880 [26]
Pu^{3+}		0.1100 [26]
Pu^{4+}		0.0960 [26]
Am^{3+}		0.1090 [27]
Am^{4+}		0.0950 [27]

ratios was from 1.948 to 2.000. The difference between the O/M ratio dependencies measured by Duriez and that measured in this study is shown in Fig. 6(a) and is slight. Thus, it is considered that the influence of Am addition on O/M ratio dependencies of A values is small.

3.3. Intrinsic lattice thermal resistivity

In the studies on thermal conductivity of oxide fuels, many authors [2,4,11,21,22] have used the following Liebfried-Schlömann relationship to explain the intrinsic lattice thermal resistivity:

$$BT = \frac{\gamma^2 T}{\left[\frac{24}{10}4^{1/3}\left(\frac{h}{k}\right)^3 \overline{M}\overline{V}^{1/3}\theta^3\right]}, \tag{16}$$

where γ is the Grüneisen constant, h the Planck's constant, k the Boltzmann constant, $\overline{M}$ the average atomic mass of the host lattice site, $\overline{V}$ the average atomic volume, and θ the Debye temperature.

It has been reported by Gibby [2] and Duriez et al. [11] that the B values predicted by using Eq. (16) were a third or fourth of experimental values. As shown in both these studies, the relative ratio of B_1 value for compound **1** to B_2 value for compound **2** can be expressed by the following equation, based on the Lindeman relationship between θ and melting temperature:

$$\frac{B_2}{B_1} = \left(\frac{M_2}{M_1}\right)^{1/2}\left(\frac{a_2}{a_1}\right)^2\left(\frac{T_{M1}}{T_{M2}}\right)^{3/2}\left(\frac{\gamma_2}{\gamma_1}\right), \tag{17}$$

where M_i, a_i, T_{Mi} and γ_i are the molecular weight, the lattice parameter, the melting point and the Grüneisen constant for compound i, respectively.

For the estimation of B value of hypostoichiometric Am–MOX, we assumed that compounds **1** and **2** in Eq. (17) are stoichiometric and hypostoichiometric Am–MOXs. As pointed out by Gibby [2] and Duriez et al. [11], the γ value of hypostoichiometric Am–MOX was assumed to be the same as that of stoichiometric Am–MOX, and thus $\gamma_1/\gamma_2 = 1$. The lattice parameter a_1 was measured as shown in Fig. 1. The lattice parameter a_2 was predicted as mentioned in the explanation of Eq. (2) [15], and can be expressed as $da/dx = 24.8 \times 10^{-12}$ m. The ratio of melting points in Eq. (17), T_{M1}/T_{M2}, was estimated from the experimental data on the melting points of $(U_{0.6}Pu_{0.4})O_{2-x}$ obtained by Kato et al. [25,28], assuming that the Pu content does not affect the O/M ratio dependency of melting points of MOX.

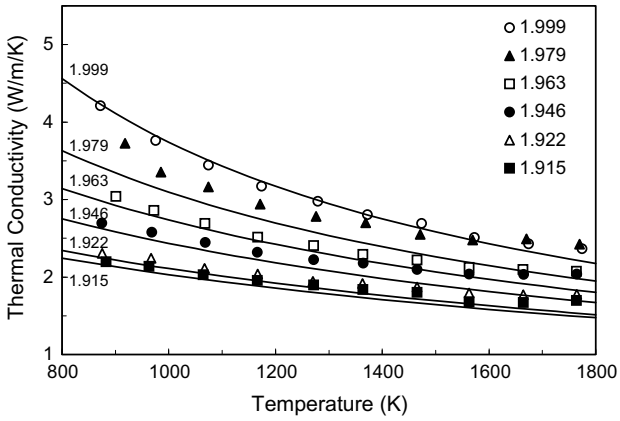

Fig. 7. Comparison between the experimental and calculated thermal conductivities. Marks are the thermal conductivities evaluated from the experimental data. Solid lines are the thermal conductivities calculated theoretically.

The B values evaluated theoretically are shown as a function of O/M ratio in Table 5 and Fig. 6(b). The B values obtained experimentally and those calculated by using Kato's data decrease with increasing x, although the gradients are different. The calculated B values agree with the experimental B values in the O/M ratio region of $x < 0.04$, but there are slight differences between both values in the O/M ratio region of $x > 0.04$. The dependency of B values on O/M ratio obtained in this study was compared with the ones of (U, Pu)O_{2-x} reported by Duriez et al. [11]. The difference between both the O/M ratio dependencies is slight as shown in Fig. 6(b). Thus, it is considered that the change of O/M ratio dependency of B values caused by Am addition is small.

Fig. 7 shows the comparison of thermal conductivities experimentally obtained with those calculated using A and B values derived from Eqs. (5)–(17). The agreements between both the experimental and the calculated thermal conductivities are good in the near-stoichiometric specimen, but the former values are slightly larger than the latter values in hypostoichiometric specimens.

4. Conclusions

The thermal conductivities of $(U_{0.68}Pu_{0.30}\text{-}Am_{0.02})\text{-}O_{2.00-x}$ solid solutions ($x = 0.00$–0.08) were measured by the laser flash method in the temperature range from 900 to 1773 K. The obtained values were normalized to 100% of the theoretical density by using the modified Maxwell–Eucken relationship.

The thermal conductivities could be expressed in the temperature region 900–1400 K by the hyperbolic equa-

tion, $\lambda = (A + BT)^{-1}$ derived from the classical phonon transport model. The A values increased linearly with increasing x, while B values decreased slightly with increasing x and the dependencies of their values on O/M ratios are summarized as follows:

$$\lambda_0 = 1/(A + BT),$$
$$A(x) = 3.31 \times x + 9.92 \times 10^{-3}\ (\mathrm{mK/W}),$$
$$B(x) = (-6.68 \times x + 2.46) \times 10^{-4}\ (\mathrm{m/W}).$$

The dependency of A values on O/M ratios was theoretically evaluated, based on the Ambegaoker's theory of phonon interaction with lattice defects. The experimental values showed a good agreement with the theoretical ones by assuming that the lattice strain parameter ε was 49.

The dependency of B values on O/M ratios was also evaluated by the Liebfried–Schlömann relationship for the intrinsic phonon resistivity. Both the experimental and the theoretical B values agreed with each other in the O/M ratio region of $x < 0.04$, but the theoretical B values were larger than the experimental ones in the O/M ratio region of $x > 0.04$.

The O/M ratio dependencies of A and B values obtained in this study were compared with the ones of $(U,Pu)O_{2-x}$ reported by Duriez et al. [11], and then it was concluded that the Am addition into $(U,Pu)O_{2-x}$ gives no significant effect on the O/M ratio dependencies of A and B values.

Acknowledgements

We acknowledge the collaboration of Messers. H. Uno, S. Shinohara, M. Shinada, M. Kowata, T. Tamura, H. Sugata, T. Sunaoshi, M. Kuwana, K. Shibata and H. Sato in sample preparation and analyses. Special thanks are also given to Emeritus Professor of Kyushu University, Dr H. Furuya for valuable discussions.

References

[1] J.C. VanCraeynest, J.C. Weilbacher, CEA-R-3488, 1968.
[2] R.L. Gibby, J. Nucl. Mater. 38 (1971) 163.
[3] J.C. Weilbacher, CEA-R-4572, 1974.
[4] S. Fukushima, T. Ohmichi, A. Maeda, M. Handa, J. Nucl. Mater. 116 (1983) 287.
[5] J.M. Bonnerot, CEA-R-5450, 1988.
[6] A.B.G. Washington, UK Atomic Energy Authority, TRG R-2236, 1973.
[7] J.H. Harding, D.G. Martin, J. Nucl. Mater. 166 (1989) 223.
[8] Y. Philipponneau, J. Nucl. Mater. 188 (1992) 194.
[9] P.G. Lucuta, H.I. Matzke, I.J. Hastings, J. Nucl. Mater. 232 (1996) 166.
[10] C.R. Ronchi, J. Appl. Phys. 85 (1999) 776.
[11] C. Duriez, J.P. Alessandri, T. Gervais, Y. Philipponneau, J. Nucl. Mater. 277 (2000) 143.
[12] D.G. Martin, J. Nucl. Mater. 110 (1982) 73.
[13] J.J. Carbajo, G.L. Yoder, S.G. Popov, V.K. Ivanov, J. Nucl. Mater. 299 (2001) 181.
[14] K. Morimoto, M. Kato, M. Ogasawara, M. Kashimura, T. Abe, J. Alloys Comp., in press.
[15] M. Kato, H. Uno, T. Tamura, K. Morimoto, K. Konashi, Y. Kihara, in: Proceedings of the Eighth Actinide Conference, Actinides 2005, Manchester, UK, 2005, p. 367.
[16] T. Baba, A. Cezairliyan, Int. J. Thermophys. 15 (1994) 343.
[17] E.H.P. Cordfunke, R.J.M. Konings, Thermochemical Data for Reactor Materials and Fission Products, North-Holland, Amsterdam, 1990, p. 35.
[18] V. Ambegaoker, Phys. Rev. 114 (1959) 488.
[19] B. Abeles, Phys. Rev. 131 (1963) 1906.
[20] M. Osaka, I. Sato, T. Namekawa, K. Kurosaki, S. Yamanaka, J. Alloys Comp. 397 (2005) 110.
[21] S. Ishimoto, M. Hirai, K. Ito, Y. Korei, J. Nucl. Sci. Technol. 31 (8) (1994) 796.
[22] M. Amaya, M. Hirai, T. Kubo, Y. Korei, J. Nucl. Mater. 231 (1996) 29.
[23] B.T.M. Willis, Proc. Roy. Soc. (London) A274 (1963) 134.
[24] R.E. Latta, R.E. Fryxel, J. Nucl. Mater. 35 (1970) 195.
[25] M. Kato, K. Morimoto, H. Sugata, K. Konashi, M. Kashimura, T. Abe, J. Nucl. Mater. 373 (2008) 237.
[26] T. Ohmichi, S. Fukushima, A. Maeda, H. Watanabe, J. Nucl. Mater. 102 (1981) 40.
[27] R.D. Shanon, Acta Crystallogr. A32 (1976) 751.
[28] M. Kato, K. Morimoto, H. Sugata, K. Konashi, M. Kashimura, T. Abe, Trans. Am. Nucl. Soc. 96 (2007) 193.